AMSI VACATION RESEARCH SCHOLARSHIPS 2022–23

SET YOUR SIGHTS ON RESEARCH THIS SUMMER

Effective magnetic properties of composites

Anna Carpenter

Supervised by Dr Karen Livesey

University of Newcastle

28 February 2023

AMSI AUSTRALIAN MATHEMATICAL SCIENCES INSTITUTE

Abstract

Composite metamaterials with magnetic nanoparticle inclusions have effective electromagnetic properties distinct from that of their constituent materials. This is because boundary conditions emergent from Maxwell's equations must be satisfied at each material interface. Many approaches have been developed to calculate effective or average magnetic permeability of composites, but most theories do not couple various components of the permeability tensor and treat it instead as a scalar quantity. Here, the complex, effective permeability tensor is found numerically by solving Maxwell's equations using a finite-difference algorithm. The frequency-dependence of the result is explored for composite systems compared to bulk magnets. In particular, we explore how the resonant frequency changes as a result of changing the shape of the inclusions in a composite. The importance of including off-diagonal effects in calculations of the effective permeability tensor is also explored. This project contributes to understanding the frequency-dependence of the permeability, and is important for chemists, physicists and engineers in the design of electromagnetic shielding materials and the overall interpretation of macroscopic effects of microwave radiation impinging on such materials.

1 Introduction

A composite material is made up of two or more constituent materials, each with distinct physical properties. By combining the constituents, we develop materials that do not exist in nature that are desired for application. For example, materials are sought that will absorb electromagnetic radiation. Key emergent areas are in medical devices and electric vehicle motor design [1], as well as radar shielding in stealth aircraft. [2] An example of an electromagnetic shielding composite consists of a flexible and lightweight host material interspersed with a small volume-fraction of magnetic inclusions. These inclusions have the capacity to absorb electromagnetic frequencies across a range of bandwidths.

The magnetic permeability $\overleftrightarrow{\mu}$ describes how easily the system becomes magnetised in response to an applied magnetic field $\mathbf{H}$. It is key for understanding electromagnetic absorption and so is the quantity that we are interested in calculating for composites in this project.

In a bulk ferromagnetic material magnetised along the z-direction (see Figure 1 for a graphic of the material's geometry), with external static magnetic field $\mathbf{H}$ applied parallel to the magnetisation $\mathbf{M}$, the permeability takes the tensor form

$$\overleftrightarrow{\mu} = \begin{pmatrix} \mu_{xx} & \mu_{xy} & 0 \\ -\mu_{xy} & \mu_{yy} & 0 \\ 0 & 0 & 1 \end{pmatrix}. \tag{1}$$

Note that this tensor is frequency dependent. In other words, if a magnet is driven at a different frequency by electromagnetic radiation, it will have a different response.

The frequency-dependent components of the tensor can be found by solving the Landau-Lifshitz-Gilbert equation

$$\frac{\mathrm{d}\mathbf{M}}{\mathrm{d}t} = -|\gamma|\left(\mathbf{M} \times \mathbf{H}_{\mathbf{total}}\right) + \frac{\alpha}{\mathbf{M}}\left(\mathbf{M} \times \frac{\mathrm{d}\mathbf{M}}{\mathrm{d}t}\right), \tag{2}$$

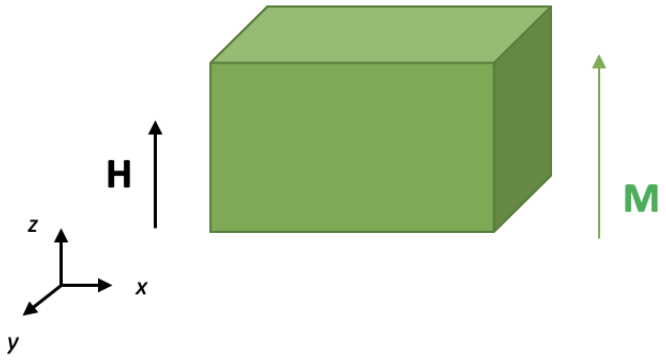

Figure 1: Geometry of a bulk ferromagnetic material magnetised in the z-direction, with $\mathbf{H} \parallel \mathbf{M}$.

which is the equation governing magnetisation dynamics. Here, $\mathbf{H_{total}} = \mathbf{H} + \mathbf{h}(t)$ is the total applied magnetic field consisting of a static part along the z direction and an oscillating driving field $\mathbf{h}(t)$ due the electromagnetic wave, in the $x-y$ directions (see Figure 1). In Equation (2), note that α is the Gilbert damping coefficient and γ is the gyromagnetic ratio. Evaluating all four of the $\overleftrightarrow{\mu}$ component expressions for a bulk ferromagnetic material is outside of the scope of this report and results are given without derivation. The on-diagonal component of the permeability tensor is found to be [3]

$$\mu_{xx} = \mu_{yy} = \frac{|\gamma|\, M(\omega_0 - \alpha i\omega)}{-\omega^2 + (\omega_0 - \alpha i\omega)^2} + 1, \tag{3}$$

where ω is the angular driving frequency of the impinging electromagnetic field $\mathbf{h}$, and $\omega_0 = \gamma H$ is the resonant Larmor frequency for magnetisation precession.

It is clear from inspection of Equation (3) that $\overleftrightarrow{\mu}$ is complex-valued. The frequency-dependence of the permeability also is seen - when the frequency ω of the impinging radiation approaches the precessional Larmor frequency of the system ω_0, the denominator of Equation (3) shrinks and the resulting on-diagonal permeability component grows very large. [3] It is around these peaks that the magnetisation can be excited by incident electromagnetic radiation most easily and energy can be absorbed strongly by the material from the radiation. This phenomenon is known as "resonance." The location of the resonance in frequency is essential to quantify for shielding material design. Figure 2 below displays the (a) real and (b) imaginary parts of μ_{yy} in a bulk ferromagnetic system as a function of frequency ω, according to Equation (3). Normalized units are used for the frequency so that resonance ($\omega = \omega_0$) occurs at 1 for bulk materials. The plot is generated using $\alpha = 0.01$ and $M/H = 10$.

In a composite, where ferromagnetic inclusions are placed within a non-magnetic host material, the magnetic permeability of the whole system is not immediately known. For example, the resonant frequency shifts from $\omega/\omega_0 = 1$. This is because composites have effective electromagnetic properties distinct from that of their constituent materials, emergent from the need for boundary conditions from Maxwell's equations to be satisfied at each material interface. [4] An additional level of intricacy is introduced when the complex nature of the

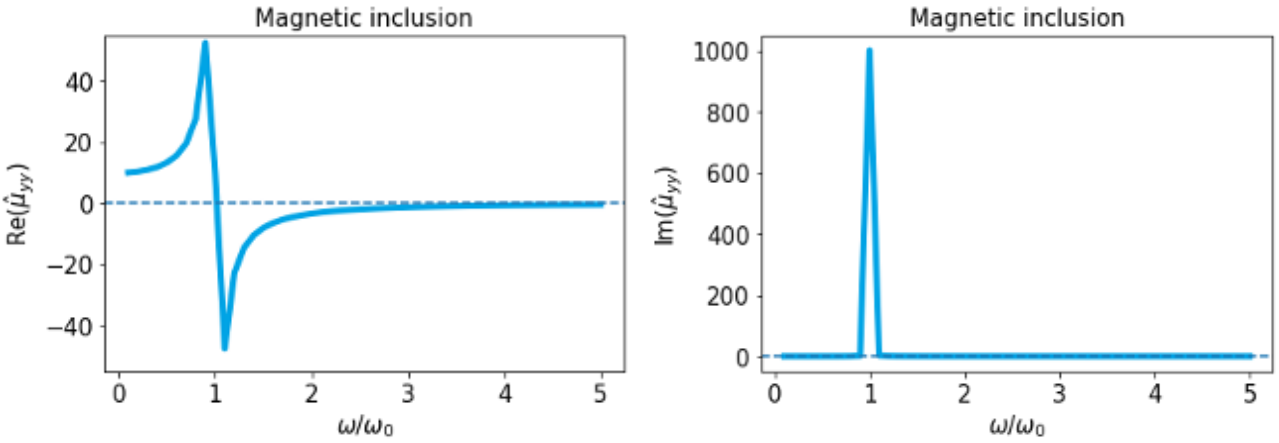

Figure 2: (a) Real and (b) imaginary parts of μ_{yy} for a bulk ferromagnetic material over a dimensionless frequency range, according to Equation (3). Here, $\alpha = 0.01$ and $M/H = 10$.

effective permeability *tensor* (from here, referred to as $\overleftrightarrow{\mu}^{eff}$) is taken into account. Surprisingly, while many approaches have been developed to calculate composite $\overleftrightarrow{\mu}^{eff}$, many of these evaluate permeability assuming the various tensor components do not influence each other, [5] and this is simply not true. [6]

A generalisation of Stroud's effective-medium approximation (EMA) for the conductivity tensor of a randomly heterogenous medium can be used to treat the permeability tensor. In other words, $\overleftrightarrow{\mu}^{eff}$ is analytically found using this approximation, in a way that honours the anisotropy of the system. [6, 7] Stroud's method works by solving a set of self-consistent matrix equations, and allows one to find the effective permeability tensor of the composite material with respect to changing frequencies across the microwave regime. However, Stroud's method makes several approximations, and breaks down when there is a large fraction of inclusions inside a host material. Therefore, numerical solutions are needed to check its validity.

The core motivation of this project, then, is to calculate the effective permeability tensor $\overleftrightarrow{\mu}^{eff}$ using a numerical scheme, free of approximations present in Stroud's EMA method. [6] This is achieved by solving Maxwell's equations using a finite-difference algorithm in Python for a two-dimensional (2D), randomly heterogenous composite system. This report covers the derivation of the algorithm on a $n \times n$ grid, the implementation of the algorithm to find $\overleftrightarrow{\mu}^{eff}$, and key results found by running the algorithm over a range of applied frequencies.

Statement of Authorship

All derivations presented in this report have been developed by the author, Anna Carpenter, based on ideas developed by Dr Karen Livesey and in consultation with Professor Robert Camley. The author acknowledges that this project springboards off work completed by Genevieve Godec, a previous student of Dr Livesey's, for *real*-valued, scalar effective permittivities of composite materials. [4] The general structure of the algorithm and

a function outlining conditions for the random placement of inclusion blocks on a 2D grid have been written based off Livesey's Mathematica code, but all other extensions to *complex*-valued, tensor permeabilities in Python for the purposes of this project are the sole work of the author.

2 Geometry of grid system

The geometry of the problem is shown in Figure 3. There exists a 2D grid to represent the composite material, comprising a non-magnetic host material (white) and small, square inclusions of some ferromagnetic material (blue). The material is considered to be uniform along the z-direction, meaning that the 2D square inclusions in the grid correspond physically to long rods of inclusion material extending into the page.

We treat the system as being periodic in x, and bounded on the top and bottom. This allows constant potential values of U to be fixed at these boundaries, simulating the effect of a uniformly applied magnetic field in the y-direction. The choice of square inclusions, as opposed to circular, was made for model simplicity on a Cartesian grid - however, square inclusions have been shown to have the same overall effect as circular inclusions. [8]

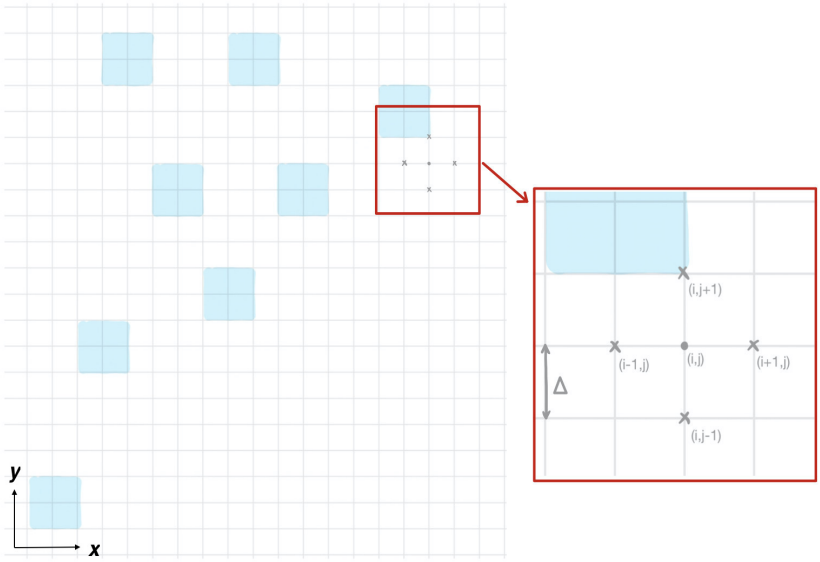

Figure 3: A 2D geometry of the host material (white) and square inclusions (blue) with a different magnetic permeability. Part of the geometry is magnified to the right to show the labelling of grid-points at and around (i,j).

The magnetostatic potential $U^{i,j}$ is defined at each grid point (i,j), with i corresponding to the x-coordinate and j corresponding to the y-coordinate. This means that one site has 4 nearest-neighbours on the grid, illustrated in Figure 3. The grid spacing is Δ, chosen such that grid points lie at the vertices of any inclusions placed on the grid. This is a choice, again, made for computational simplicity, but if desired the position of

inclusions could be modified to be considered 'between' points (using a Yee grid [9] or similar).

Magnetic permeability values are defined at the square spaces formed between the grid vertices. Two $n\times n$ arrays holding the on-diagonal and off-diagonal permeability components of the two distinct materials keep the values at the same spaces in whatever inclusion arrangement is being treated. The total 2D space, then, contains $2n\times 2n$ permeability and $n\times(n+1)$ potential values, where $n\Delta$ is the dimensionless length of one side of the grid.

Inclusions are placed randomly in the grid by generating a set of (i,j) coordinates that fall within the space, selected from a confined range of integer values using the `random` library in Python. This random point corresponds to the bottom-left vertice of the whole inclusion. If filling a full-size square array of the desired inclusion area does not overlap with existing inclusions on the grid or spill over the vertical boundaries, the block is placed. Otherwise, a new random coordinate is selected, repeating until the desired amount of inclusions are placed. We have considered inclusions that do not touch because the shape of the inclusions becomes effectively very different if they were to touch. This alters the magnetic fields generated by magnetisation of the inclusions (*demagnetising* fields), and would have flow-on effects for our algorithm in the calculation of $\overleftrightarrow{\mu}^{eff}$.

3 Algorithm for potential U

Maxwell's equations are a set of four differential equations that are fundamental to the study of physics, particularly in the areas of electromagnetism and optics. Here, a subset of these equations are discretised using a finite-difference approximation for the derivatives, and then applied to every (i,j) grid-point to write a linear equation relating each potential $U^{i,j}$ to a sum of its' neighbours. The intuition behind the approach follows algorithms commonly used to solve second-order differential equations (such as Laplace's equation) in uniform materials, [10] although here the neighbouring points contribute unequal amounts to each potential point $U^{i,j}$. The derivation of Nagel [11] for electrostatic problems has been a key reference for development of this report's algorithm, due to its detailed approach for dealing with nonuniform electromagnetic properties. However, we have extended its approach here to be applied to a *magnetostatic* problem with *tensor* quantities.

The equation for the magnetic flux density $\mathbf{B}$ in SI units is

$$\mathbf{B} = \mu_0(\mathbf{H} + \mathbf{M}) \tag{4}$$

where μ_0 is the vacuum permeability, $\mathbf{H}$ is the magnetic field, and $\mathbf{M}$ is the magnetisation. For linear magnetic materials, one can rewrite Equation (4) as

$$\begin{aligned}\mathbf{B} &= \mu_0(\mathbf{H} + \overleftrightarrow{\chi}\mathbf{H}) \\ &= \overleftrightarrow{\mu}\mathbf{H}\end{aligned} \tag{5}$$

where $\overleftrightarrow{\chi}$ is the magnetic susceptibility tensor and $\overleftrightarrow{\mu}$ is the permeability tensor of the material. Note that $\overleftrightarrow{\mu} = \mu_0(1+\overleftrightarrow{\chi}) = \mu_0\overleftrightarrow{\mu}_r$, where $\overleftrightarrow{\mu}_r$ is the unitless relative permeability tensor. This takes the form presented earlier

in Equation (1) and Figure 1 for ferromagnetic materials magnetised along the z-direction, which matches the configuration of the composite systems treated in this report.

Now the discretisation of Maxwell's magnetostatic equations is discussed. In a system with no free charges or currents, Ampére's Law simplifies to $\nabla \times \mathbf{H} = 0$. This implies that $\mathbf{H}$ is a conservative vector field, and so can be written as the gradient of a potential function $U(\mathbf{r})$, namely,

$$\nabla \times \mathbf{H} = 0 \implies \mathbf{H} = -\nabla U. \tag{6}$$

This result, paired with Equation (5) can be substituted into Gauss' law for the magnetic field in order to find an equation for U according to

$$\begin{aligned} 0 &= \nabla \cdot \mathbf{B} \\ &= \nabla \cdot (\overleftrightarrow{\mu}\mathbf{H}) \\ &= -\nabla \cdot (\overleftrightarrow{\mu}\nabla U). \end{aligned} \tag{7}$$

Equation (7) can then be solved everywhere on the grid-space to find the magnetostatic potential U over all (i,j). It is essential that $\overleftrightarrow{\mu}$ is not pulled out of the brackets in Equation (7), since it depends on position and must stay where it is to derive the correct finite-difference algorithm.

To discretise Equation (7), one can first integrate both sides over a square area $\Omega_{i,j}$ centred at the point of interest (i,j), with side-length Δ. A visualisation of this is presented in Figure 4. The divergence theorem can then be applied to reduce the area integral to a line integral as per Nagel's application [11]

$$0 = \int_{\Omega_{i,j}} \nabla \cdot (\overleftrightarrow{\mu}\nabla U) da = \oint_{C_{i,j}} [\overleftrightarrow{\mu}\nabla U] \cdot d\hat{n}, \tag{8}$$

such that $C_{i,j}$ is the square path that encloses area $\Omega_{i,j}$ and $\hat{n}$ is the unit vector normal to $C_{i,j}$. We then find a finite-element approximation for this path integral by just summing the four parts of $C_{i,j}$ individually, moving towards the form of a linear equation for each magnetic potential $U_{i,j}$ on the grid.

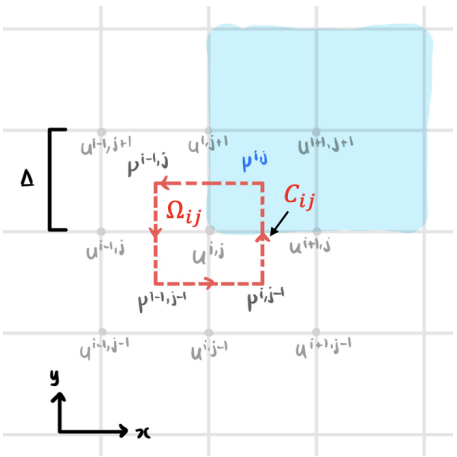

Figure 4: The square contour (dotted line) centred on site of interest (i,j) used to discretise Equation (7). $\Omega_{i,j}$ is the area of side-length Δ and $C_{i,j}$ is the counter-clockwise contour path.

For illustrative purposes, we will step through deriving a finite-difference expression for the right-hand path of $C_{i,j}$. It is clear from the coordinate axes defined in Figure 4 that the unit vector $\hat{n}$ points in the positive x direction. We can denote here that $\hat{n} \parallel \hat{x}$. We then have

$$\begin{aligned}\int_{right} [\overleftrightarrow{\mu}\nabla U] \cdot d\hat{n} &= \int_{right} [\overleftrightarrow{\mu}\nabla U] \cdot \hat{x} dy \\ &= \int_{(j-\frac{1}{2})\Delta}^{(j+\frac{1}{2})\Delta} \left(\mu_{xx}\frac{\partial U}{\partial x} + \mu_{xy}\frac{\partial U}{\partial y}\right) dy,\end{aligned} \tag{9}$$

which represents a quarter of the total integral along the path C_{ij}.

Finite-difference expressions for the partial derivatives $\frac{\partial U}{\partial x}$ and $\frac{\partial U}{\partial y}$ involve the nearest-neighbours to site (i,j). The right path is further split into two pieces so that the derivatives can be evaluated around the square with permeability $\overleftrightarrow{\mu}^{i,j}$ and the one with $\overleftrightarrow{\mu}^{i,j-1}$ (see Figure 4). The result is

$$\begin{aligned}\int_{right} [\overleftrightarrow{\mu}\nabla U] \cdot d\hat{n} \approx \frac{\Delta}{2}&\left(\mu_{xx}^{i,j-1}\frac{U^{i+1,j}-U^{i,j}}{\Delta} + \mu_{xy}^{i,j-1}\frac{U^{i,j}+U^{i+1,j}-U^{i,j-1}-U^{i+1,j-1}}{2\Delta}\right) \\ &+ \frac{\Delta}{2}\left(\mu_{xx}^{i,j}\frac{U^{i+1,j}-U^{i,j}}{\Delta} + \mu_{xy}^{i,j}\frac{U^{i,j+1}+U^{i+1,j+1}-U^{i,j}-U^{i+1,j}}{2\Delta}\right).\end{aligned} \tag{10}$$

The superscripts denote either the squares between grid points where permeability μ is defined, or the grid points themselves where potential U is defined. A visualisation of this notation is provided in Figure 4.

Following the same derivation process, the remaining three paths for $C_{i,j}$ can be approximated using the finite-difference method. The four paths are summed together to obtain a discrete algorithm for the magneto-static potential at (i,j) which represents exactly the same physics as the continuous partial differential equation defined in Equation (7). After some cancellation, we get

$$\begin{aligned}U^{i,j} = \Big\{&U^{i+1,j}(\mu_{xx}^{i,j} + \mu_{xx}^{i,j-1} + \mu_{xy}^{i,j-1} - \mu_{xy}^{i,j}) \\ &+ U^{i-1,j}(\mu_{xx}^{i-1,j} + \mu_{xx}^{i-1,j-1} + \mu_{xy}^{i-1,j} - \mu_{xy}^{i-1,j-1}) \\ &+ U^{i,j+1}(\mu_{xx}^{i,j} + \mu_{xx}^{i-1,j} + \mu_{xy}^{i,j} - \mu_{xy}^{i-1,j}) \\ &+ U^{i,j-1}(\mu_{xx}^{i,j-1} + \mu_{xx}^{i-1,j-1} + \mu_{xy}^{i-1,j-1} - \mu_{xy}^{i,j-1})\Big\} \\ &\{-2(\mu_{xx}^{i,j} + \mu_{xx}^{i,j-1} + \mu_{xx}^{i-1,j} + \mu_{xx}^{i-1,j-1})\}^{-1} \\ &.\end{aligned} \tag{11}$$

Equation (11) can be rearranged to form a weighted average sum over the four nearest neighbours to $U^{i,j}$, namely

$$U^{i,j} = \alpha U^{i+1,j} + \beta U^{i-1,j} + \gamma U^{i,j+1} + \xi U^{i,j-1}, \tag{12}$$

where the weighting coefficients α, β, γ and ξ involve combinations of both on- and off-diagonal components of the permeability tensor in the four neighbouring squares.

4 Solving for $\overleftrightarrow{\mu}^{eff}$

Equation (12) (derived above) is written for every $U^{i,j}$ point on our $n \times n$ grid. This sets up a system of n^2 linear equations. At the vertical boundaries ($U^{i,0}$ at the bottom and $U^{i,n-1}$ at the top) fixed values of the scalar

potential are assumed, namely U_{bottom} and U_{top} respectively. The choices of j match the indexing convention in Python, the programming language used to solve the set of linear equations. The resulting system of equations can be solved directly through matrix inversion for smaller systems. However, Python's `linalg` package in the `numpy` library can be used to output a solution for larger systems. An $n^2 \times n^2$ sparse matrix of weighted coefficients from Equation (12), multiplies by a column vector containing all the $U^{i,j}$ to give a column vector containing the vertical boundary conditions. To give an example of the calculation time, for a 120 × 120 grid system, it takes approximately 130 seconds to write and solve a 14,400 × 14,400 matrix equation. Smaller systems, such as those on an 80 × 80 grid (generating a 6400 × 6400 matrix equation), could be solved in approximately 10 seconds.

Once the potential $U^{i,j}$ is found for all grid-points, the x- and y-components of the magnetic field strength $\mathbf{H}$ can be found by also using a finite-difference approximation of the derivative. This is because $\vec{H} = -\nabla U$ according to Ampére's Law in Equation (6). Using the grid geometry given in Figure 4, the y-component of the magnetic field is calculated as

$$H_y^{i,j} = -\frac{\partial U}{\partial y} = -\frac{U^{i+1,j+1} + U^{i,j+1} - U^{i+1,j} - U^{i,j}}{2\Delta}. \tag{13}$$

A similar equation can be used to find the horizontal component $H_x^{i,j}$. The magnetic flux density $\mathbf{B}$ can also be found everywhere on the grid with a modification to Equation (5). One finds the vertical component of the *local* magnetic flux density to be

$$B_y^{i,j} = \overleftrightarrow{\mu}^{i,j} H_y^{i,j} \tag{14}$$

Finally, the components of the effective permeability tensor can be found by summing up all the *local* fields to form global average fields. Then, the on-diagonal component of the effective permeability is

$$\begin{aligned} \mu_{yy}^{eff} &= \frac{\langle B_y \rangle}{\langle H_y \rangle} \\ &= \frac{\sum_{all\ i,j} B_y^{i,j}}{\sum_{all\ i,j} H_y^{i,j}}, \end{aligned} \tag{15}$$

where the angled brackets denote an average field component.

Similary, the off-diagonal component of the effective permeability is

$$\begin{aligned} \mu_{xy}^{eff} &= \frac{\langle B_x \rangle}{\langle H_y \rangle} \\ &= \frac{\sum_{all\ i,j} B_x^{i,j}}{\sum_{all\ i,j} H_y^{i,j}}. \end{aligned} \tag{16}$$

As a reader may infer from earlier discussion, the bulk of the algorithm's runtime comes from writing and solving the system of linear equations. A method, then, to calculate quick approximations of $\overleftrightarrow{\mu}^{eff}$ for test systems involves fixing the volume fraction of inclusions and iterating through several randomly generated spatial distributions of the inclusions within the host material. By taking the average of each iteration's output $\overleftrightarrow{\mu}^{eff}$, variation in the result due to the way inclusion blocks are placed in a smaller grid is minimised. One can gain a feeling for the system's $\overleftrightarrow{\mu}^{eff}$ quickly in this way. For larger n, $\overleftrightarrow{\mu}^{eff}$ is not as dependent on the placement of inclusions, indicating that the system is large enough to simulate results of a real material.

5 Effective permeability of composites

To illustrate the general results, we will present some fields calculated for an 80 × 80 composite material grid and show how these fields satisfy boundary conditions emergent from Maxwell's equations. The resonance behaviour for a composite system will also be presented and compared to earlier results for a bulk ferromagnet (seen in Figure 2).

The parameter used in this report to represent the volume fraction of magnetic inclusions is the filling fraction f. This is the fraction of total material 'filled' by inclusions. For example, an 80 × 80 grid with 15 8×8 inclusions has $f = 0.15$. A grid of this size has been chosen to present a clearer visualisation of the field behaviour below in Figure 5.

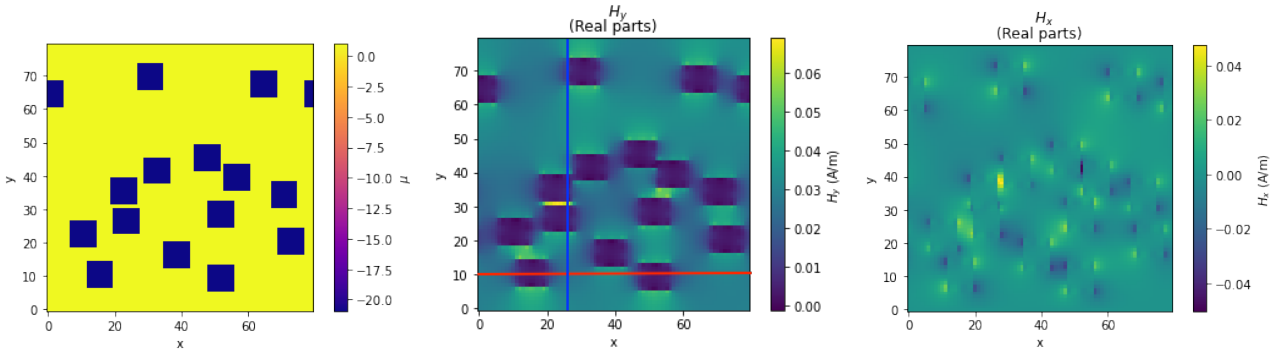

Figure 5: Relative permeability and field behaviour in an 80 × 80 composite grid with f=0.15. Colourbars on the right of each plot indicate relevant magnitudes. Panel (a) shows the real part of the local permeability, with the inclusions clearly shown as blue blocks on a yellow background. Panel (b) shows the real part of the local H_y and (c) shows the real part of local H_x. The blue and red lines in panel (b) denote the position of cross-sections that are examined in Figure 6.

Figure 5(a) shows the placement of 15 inclusion 'blocks' in one randomly generated configuration. The shading in the graph corresponds to the real part of the local μ_{xx} for the initial relative permeability allocated to the two constituent materials. For the non-magnetic host, $\mathrm{Re}(\mu_{xx}) = \mu_{xx} = 1$. At the ferromagnetic inclusion sites, $\mathrm{Re}(\mu_{xx})$ matches the expression presented above in Equation (3) for materials magnetised in the z-direction (into the page). Notice the periodic boundary conditions in x being applied at around y=61, where the block effectively 'wraps around' to the left-hand side. Further, none of the square inclusions are touching each other.

Density plots for the magnetic field strength components H_y (Figure 5(b)) and H_x (Figure 5(c)) are also presented. The behaviour of the fields is clearly a function of position, with respect to the changing permeabilities between host and inclusion in Figure 5(a). In Figure 5(b), there is a uniform background with distortions in H_y at the inclusion sites. By both visual inspection and by taking a vertical cross-section (see x=25 in Figure 6(a)), it is clear that there are abrupt field discontinuities at vertical interfaces. This is such that the general boundary condition from solving Gauss' law at a material interface is satisfied at the top and bottom of each block. The

general rule, derived in [12], states that **B** components *normal* to the interface junction of two separate materials must be equal in both materials. Since $B = \mu H$, this implies that $\mu^{inc} H_y^{inc} = H_y^{host}$, over changing y. Re(H_y) inside the inclusions is smaller than in the non-magnetic host to account for this. Over changing x, the algorithm produces smoother changes in H_y as it moves between materials. A horizontal cross-section of H_y values at y=10 is plotted in Figure 6(b) to support this observation.

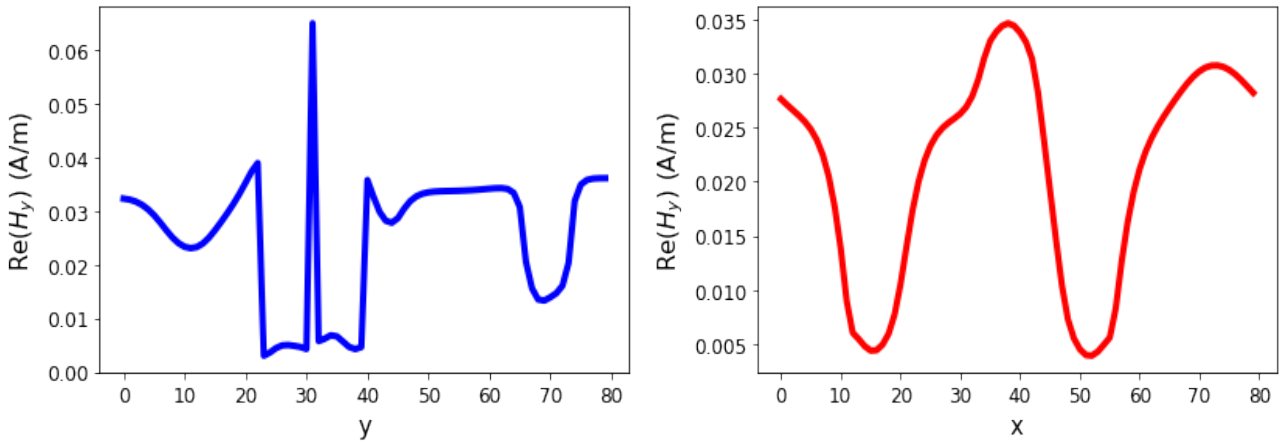

(a) (b)

Figure 6: Cross-sections of the real part of the vertical field H_y, taken along an (a) vertical and (b) horizontal line shown in the material space in Figure 5(b).

In Figure 5(c), H_x is generally zero. This makes sense, as there is no externally applied potential at the horizontal boundaries to produce a net magnetic field in the x direction (a field *is* present in the y direction from the specification of constants U_{top} and U_{bottom} as outlined in Section 3). Similar to in Figure 5(b), though, there are clearly discontinuous changes in H_x at horizontal interfaces. This change in field values is consistent with the boundary condition for components normal to the interface junction, [12] and so also makes sense physically.

The Python code was used to calculate $\overleftrightarrow{\mu}^{eff}$ for a composite system over a range of applied frequencies. In the Introduction, we explored why the resonant frequency of a composite material is not immediately known. In summary, this is due to the need to satisfy local field boundary conditions at each material interface in the system, as well as the inclusion of complex tensor permeabilities. Figure 7 shows results for the real part of μ_{yy}^{eff} in a system with volume fraction f=0.15, over a dimensionless frequency range $0.2 \leq \frac{\omega}{\omega_0} \leq 6.0$. In Figure 7a, resonance behaviour of the composite (dark line) is plotted on the same axes as that of the bulk ferromagnet (lighter line) from Figure 2 to compare scale and location of resonant frequencies. Results have also been plotted in Figure 7(b) against a version of the code which ignores off-diagonal components of $\overleftrightarrow{\mu}$ at the inclusion sites, setting them to 0 for consecutive calculations of the composite material's overall $\overleftrightarrow{\mu}^{eff}$. This was done to explore how important the treatment of off-diagonal components in the algorithm was for final calculations. A step-size of 0.1 was taken between each frequency input, with 2 iterations at each frequency run

and consecutively averaged. This was done to minimise the effect of inclusion placement on changing $\overleftrightarrow{\mu}^{eff}$, and was a method discussed at the end of the previous section to reduce the algorithm's runtime.

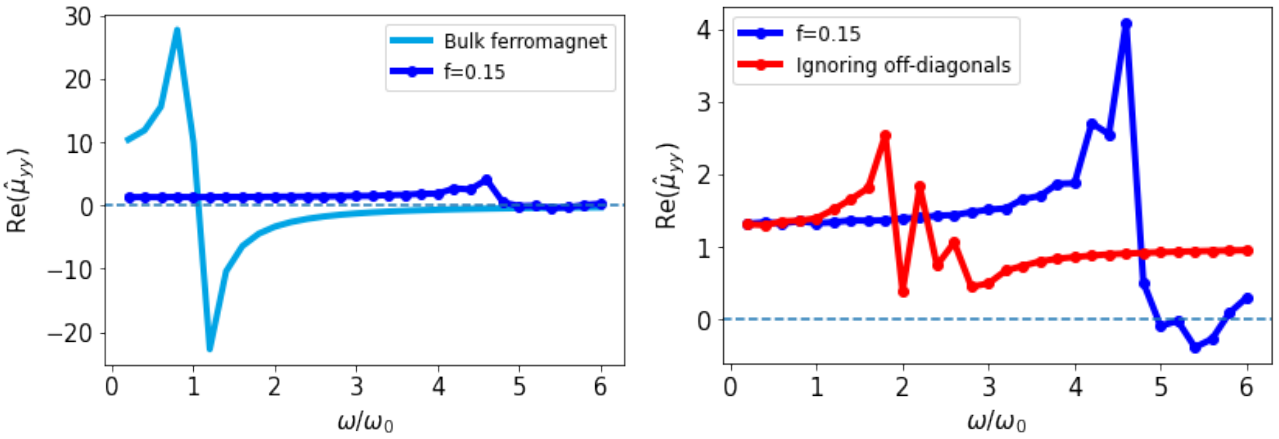

(a) (b)

Figure 7: The real part of ${\mu_{yy}}^{eff}$ for a composite 80 × 80 material over a dimensionless frequency range, with volume fraction f=0.15. Here, $\alpha = 0.01$ and $M/H = 10$. Panel (a) compares the composite result (dark line) to that of a bulk magnet (lighter line). Panel (b) compares the result to that which would occur if one ignored the coupling of off-diagonal components to the on-diagonal permeability value (red line).

The real part of ${\mu_{yy}}^{eff}$ undergoes a sign change at a certain frequency, and this frequency corresponds roughly to the resonant frequency for a given system. Figure 7(a) shows that this shifts from $\frac{\omega}{\omega_0} = 1$ in the bulk ferromagnet (lighter line) to $\frac{\omega}{\omega_0} \approx 4.6$ in the composite (dark line). The uncertainty in the answer comes mainly from the resolution uncertainty by taking frequency step-sizes of 0.1. Physically, this means that there is the greatest electromagnetic absorption by the composite when the angular driving frequency ω of the impinging electromagnetic field is about 4.6 times **greater** than the precessional frequency ω_0 of the bulk magnet. This is due to the shape anisotropy of the added inclusions, as they introduce additional effective fields on top of the external applied one, thus shifting the resonance location. This matches predictions of a shift in resonance due to shape aniostropy from analytic approximations. [6] One can also observe the decreased magnitude of the peak in a composite material compared to bulk, which makes sense as there is a smaller volume-fraction of material with absorptive capacity. The characteristic sign change denoting the resonance location is perhaps more obvious in Figure 7(b), as the range of the y-axis is more comparable to the size of ${\mu_{yy}}^{eff}$.

Finally, we consider the importance of treating off-diagonal components of $\overleftrightarrow{\mu}$ as a part of the effective permeability calculations. Figure 7(b) compares the resonance behaviour of the same f=0.15 system as before, to a series of simulations for the same filling fraction where the off-diagonal $\overleftrightarrow{\mu}$ components of the inclusions are *set to 0*. Consecutive calculations of Re(${\mu_{yy}}^{eff}$) here show a total mismatch between the resonance behaviour of this system where off-diagonal effects are ignored, and our system where anisotropy of the material is accounted for. This affirms that it is essential to account for off-diagonal permeability components when performing these

calculations, and affirms the approach taken in the design of this algorithm.

6 Discussion and Conclusion

A 2D finite-difference code was written to calculate $\overleftrightarrow{\mu}^{eff}$ for randomly heterogenous composite systems. Results show that there is a shift in resonant frequencies for composites compared to bulk magnetic materials, and that this can be explained by the shape anisotropy introduced by the inclusions. It was also confirmed that off-diagonal terms are essential for calculations of $\overleftrightarrow{\mu}^{eff}$ in composite material design, a conclusion which is supported by analytic approximations using Stroud's method. [6]

A natural continuation of this project involves extending the composite space modelled to three dimensions, a task that will involve discretising Maxwell's equations such that additional terms are introduced to the final equation for $U_{i,j}$. The algorithm could also be modified such that inclusions have magnetisation $\mathbf{M}$ in either the positive *or* negative z-direction, potentially even letting the direction of $\mathbf{M}$ be represented as a probability in order to intersect with other areas of physics like statistical mechanics. A final future direction involves optimising the code that runs the algorithm; A key area of investigation involves using sparse matrix packages in Python to improve runtime, or even investigating other programming languages.

Acknowledgements

I'd like to acknowledge the invaluable contributions of my supervisor, Dr Karen Livesey, to this project, the bulk of which (pun not intended) springboards off work completed by herself and past research students on effective permittivity finite-difference algorithms. I'd also like to thank Professor Robert Camley of the University of Colorado, Colorado Springs, for his consultation and advice on this project.

Finally, I'd like to thank my family and my partner for their unwavering support and willingness to listen to my ramblings on mathematics and physics. Perhaps unfortunately for them, I'm sure these conversations will be continuing for many years.

References

[1] K. Livesey, R. Camley, Z. Celinski, S. Maat, Magnetic shielding of 3-phase current by a composite material at low frequencies, AIP Adv. 7 (2017) 056328. doi:10.1063/1.4978702.

[2] F. Idris, M. Hashim, Z. Abbas, I. Ismail, R. Nazlan, I. Ibrahim, Recent developments of smart electromagnetic absorbers based polymer-composites at gigahertz frequencies, J. Magn. Magn. Mater 405 (2016) 197–208. doi:10.1016/j.jmmm.2015.12.070.

[3] J. Coey, Magnetism and Magnetic Materials, Cambridge University Press, 2009, Ch. 12 Applications of Soft Magnets, pp. 445–447.

[4] G. Godec, K. Livesey, Computing the effective permittivity of composite materials using a finite difference method, Am. J. Phys. 87 (6) (2019) 465–470. doi:10.1119/1.5102146.

[5] P. Queffelec, D. Bariou, P. Gelin, A predictive model for the permeability tensor of magnetized heterogeneous materials, IEEE Trans. Magn. 41 (2005) 17 – 23. doi:10.1109/TMAG.2004.837755.

[6] P. Thibaudeau, J. Tranchida, Frequency-dependent effective permeability tensor of unsaturated polycrystalline ferrites, J. Appl. Phys. 118 (5) (2015) 053901. doi:10.1063/1.4927724.

[7] J. P. Bouchaud, P. G. Zérah, Spontaneous resonances and universal behavior in ferrimagnets: Effective-medium theory, Phys. Rev. Lett. 63 (1989) 1000–1003. doi:10.1103/PhysRevLett.63.1000.

[8] K. L. Livesey, R. E. Camley, Large, tunable microwave permittivity in a liquid doped with anisotropic particles, J. Appl. Phys. 120 (5) (2016) 054503. doi:10.1063/1.4959987.

[9] K. Yee, Numerical solution of initial boundary value problems involving Maxwell's equations in isotropic media, IEEE Trans. Antennas Propag. 14 (3) (1966) 302–307. doi:10.1109/TAP.1966.1138693.

[10] A. L. Garcia, Numerical Methods for Physics, 2nd Edition, Prentice Hall, 2000.

[11] J. Nagel, Solving the generalized Poisson equation using the finite-difference method (FDM), https://my.ece.utah.edu/ẽce6340/LECTURES/Feb1/Nagel%202012%20- %20Solving%20the%20Generalized%20Poisson%20Equation%20using%20FDM.pdf (February 2012).

[12] A. Wolski, Theory of electromagnetic fields Part ii: Standing waves (June 2010).
URL https://cas.web.cern.ch/sites/default/files/lectures/ebeltoft-2010/wolski-2.pdf